BIOCHEMISTRY
including biophysical chemistry & molecular biology

Article

pubs.acs.org/biochemistry

# Constitutively Active Glutaminase Variants Provide Insights into the Activation Mechanism of Anthranilate Synthase

Felix List, Marco Bocola, Michaela C. Haeger, and Reinhard Sterner*

Institute of Biophysics and Physical Biochemistry, University of Regensburg, Universitätsstrasse 31, D-93053 Regensburg, Germany

Supporting Information

**ABSTRACT:** The glutamine amidotransferase (GATase) family comprises enzyme complexes which consist of glutaminase and synthase subunits that catalyze in a concerted reaction the incorporation of nitrogen within various metabolic pathways. An important feature of GATases is the strong stimulation of glutaminase activity by the associated synthase. To understand the mechanism of this tight activity regulation, we probed by site-directed mutagenesis four residues of the glutaminase subunit TrpG from anthranilate synthase that are located between the catalytic Cys−His−Glu triad and the synthase subunit TrpE. In order to minimize structural perturbations induced by the introduced exchanges, the amino acids from TrpG were substituted with the corresponding residues of the closely related glutaminase HisH from imidazole glycerol phosphate synthase. Steady-state kinetic characterization showed that, in contrast to wild-type TrpG, two TrpG variants with single exchanges constitutively hydrolyzed glutamine in the absence of TrpE. A reaction assay performed with hydroxylamine as a stronger nucleophile replacing water and a filter assay with radiolabeled glutamine indicated that the formation of the thioester intermediate is the rate-limiting step of constitutive glutamine hydrolysis. Molecular dynamics simulations with wild-type TrpG and constitutively active TrpG variants suggest that the introduced amino acid exchanges result in a distance reduction between the active site Cys−His pair, which facilitates the deprotonation of the sulfhydryl group of the catalytic cysteine and thus enables its nucleophilic attack onto the carboxamide group of the glutamine side chain. We propose that native TrpG in the anthranilate synthase complex is activated by a similar mechanism.

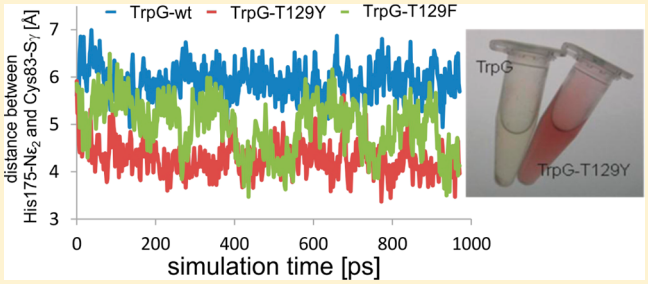


Members of the glutamine amidotransferase (GATase) enzyme family catalyze the incorporation of nitrogen during the biosynthesis of amino acids, nucleotides, and various other metabolites.[1−4] GATases consist of distinct glutaminase and synthase subunits or domains and are divided into two groups, which are differentiated by the topology of the glutaminase subunits. Whereas GATase I enzymes contain G-type glutaminases with an $\alpha/\beta$ hydrolase fold and a Cys−His−Glu catalytic triad,[5] GATase II enzymes contain glutaminases with an Ntn hydrolase fold and a crucial cysteine at the N-terminus of the polypeptide chain.[6] Both types of glutaminases generate ammonia, which is channeled to the synthase active site where it reacts with a second substrate that is specific for each GATase.[7] Importantly, in order to avoid the wasteful consumption of glutamine, the catalytic activity of the glutaminase subunit is dependent on the presence of the synthase subunit and in most cases also the synthase substrate.[8−11]

We analyzed the mechanistic basis for the functional coupling between the glutaminase subunit TrpG and the synthase subunit TrpE of anthranilate synthase (AS), which is a prototypical GATase. AS catalyzes the first step in tryptophan biosynthesis, the generation of anthranilate and pyruvate from glutamine and chorismate[12] (Figure 1). The crystal structures of the AS from *Serratia marcescens*, *Samonella typhimurium*, and *Sulfolobus solfataricus* show that the glutaminase subunit (TrpG), which adopts the triad G-type amidotransferase fold, and the synthase subunit (TrpE), which adopts a complicated $\alpha/\beta$ folding pattern, assemble to heterotetrameric $(TrpE−TrpG)_2$-complexes. Whereas the structural interactions within the functional TrpE−TrpG heterodimers are similar for the AS from the three species, the modes of assembly of the two dimers to the tetramer are different.[13−15] In spite of these comprehensive structural data, little is known about the mechanism that underlies the activation of TrpG by TrpE. In order to obtain insights into this process, we generated constitutively active TrpG variants and analyzed their reaction mechanism experimentally and by molecular dynamics (MD) simulations.

## MATERIAL AND METHODS

**Cloning of Genes and Site-Directed Mutagenesis.** The wild-type *trp*E, *trp*GD, and *trp*G genes were amplified from *T. maritima* genomic DNA with site specific primers (Table S1, Supporting Information), introducing *Nde*I and *Hin*dIII

Received: October 24, 2011
Revised: March 15, 2012
Published: March 20, 2012

ACS Publications © 2012 American Chemical Society

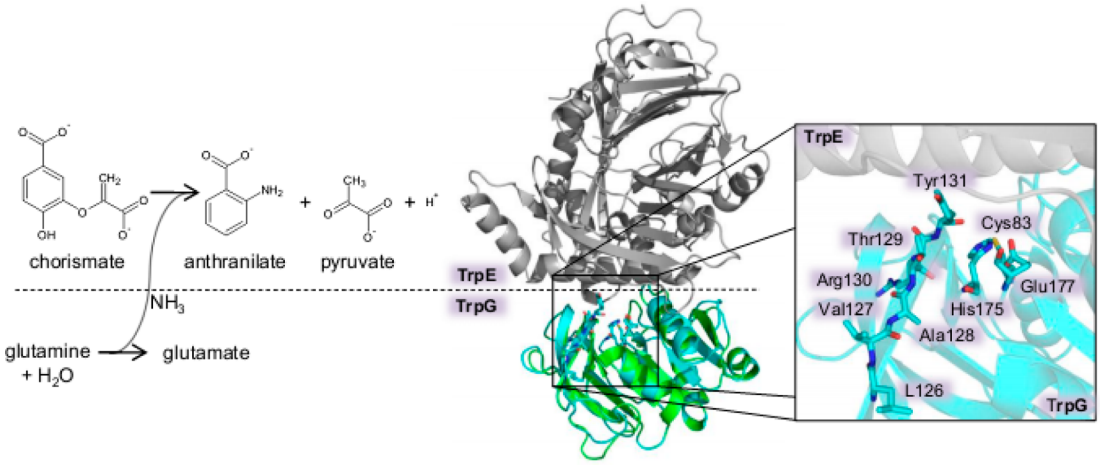


**Figure 1.** Reaction scheme and crystal structure of anthranilate synthase. Left panel: Glutamine is hydrolyzed by the TrpG subunit to glutamate. Nascent ammonia is transferred to the TrpE subunit where it reacts with chorismate to anthranilate and pyruvate. Right panel: Ribbon diagram of the homology model of TrpG from *T. maritima* (blue) generated by Swiss Model (http://swissmodel.expasy.org/) superposed on the heterodimeric TrpE (gray)−TrpG (green) AS complex from *S. solfataricus*. The amino acid stretch selected for mutation (Leu126−Tyr131) and the catalytic triad (Cys83−His175−Glu177) of TrpG are shown enlarged in ball and stick representation. The structure is shown enlarged and in stereo depiction as Figure S2.

resctriction sites for subcloning into pET28a(+) (*trp*E) or pET21a(+) (*trp*GD), and *Nde*I and *Bam*HI restriction sites for subcloning into pET11c (wild-type *trp*G). Mutations were introduced into *trp*G by overlap extension PCR[16] using the oligonucleotides shown in Table S1, and cloned into pET28a-(+) using *Nde*I and *Bam*HI sites (*trp*G-T129F, *trp*G-T129Y, and *trp*G-Y131V), or into pET21a(+) using *Nde*I and *Xho*I sites (*trp*G-L126G, *trp*G-V127Y, and *trp*G-T129A), or into pET11c using *Nde*I and *Bam*HI sites (*trp*G-L126G+V127Y+T129Y +Y131V).

**Heterologous Gene Expression and Purification of Recombinant Proteins.** Heterologous expression of plasmid-encoded *trpE*, *trpGD*, and *trpG* genes was performed in *E. coli* BL21(DE3)RIPL (*trp*E) or *E. coli* BL21(DE3)Rosetta (*trp*GD, *trp*G) (Stratagene). Expression from pET28a(+) resulted in the addition of a N-terminal hexa-histidine ($His_6$) tag, expression from pET21a(+) in the addition of a C-terminal $His_6$-tag to the recombinant protein. Ten liters (TrpE) or 2 L (TrpGD, TrpG) of Luria-Broth medium supplemented with 150 $\mu$g/mL ampicillin [pET11c and pET21a(+)] or 75 $\mu$g/mL kanamycin [pET28a(+)] were inoculated with a preculture and incubated at 37 °C. After an $OD_{600}$ of 0.6 was reached, expression was induced by adding 1 mM (TrpE) or 0.5 mM (TrpGD, TrpG) of IPTG, and growth was continued for 4 h (TrpE) or overnight (TrpG, TrpGD). Cells were harvested by centrifugation (Sorvall/RC5B, GS3, 15 min, 4000 rpm, 4 °C), washed with 50 mM potassium phosphate buffer, pH 7.5, and centrifuged again. The cell paste was resuspended in the same buffer, lysed by sonification on ice (Branson Sonifier W-250D, 4 min in 15 s intervals, 50% pulse), and centrifuged (Sorvall/RC5B, SS34, 30 min, 13 000 rpm, 4 °C) to separate the soluble from the insoluble fraction of the cell extract. The recombinant proteins were enriched from the soluble fraction by heat precipitation of the host proteins (20 min at 50 °C for TrpE, and 60 °C for TrpGD and TrpG) and centrifuged. Supernatants containing $His_6$-tagged proteins were loaded onto a nickel sepharose column [POROS MC/20 (Applied Biosystems) in the case of TrpE, and HisTrap FF crude 5 mL (GE Healthcare) in the case of TrpGD and TrpG variants carrying single residue exchanges], which had been equilibrated with 50 mM potassium phosphate pH 7.5, 300 mM NaCl, 10 mM imidazole. The column was washed with equilibration buffer. In the case of TrpE, the pH was reduced to pH 5.5 in a linear gradient as a second washing step. Bound $His_6$-tagged protein was eluted by applying a linear gradient of 1−500 mM imidazole. Fractions containing enriched TrpGD or TrpG variants were additionally loaded onto a MonoQ column (HR 16/10, 20 mL, Pharmacia), which had been equilibrated with 50 mM potassium phosphate pH 7.5. Supernatant containing wild-type TrpG or TrpG-L126G+V127Y+T129Y+Y131V without $His_6$-tag was loaded onto a MonoQ column directly after heat precipitation. The column was washed with equilibration buffer, and bound protein was eluted by applying a linear gradient of 0−1.5 M NaCl. Elution fractions containing pure protein were pooled and dialyzed extensively against 50 mM potassium phosphate pH 7.5. According to SDS−PAGE (12.5% acrylamide), all proteins were more than 90% pure. Protein concentrations were determined by measuring the absorbance at 280 nm, using a molar extinction coefficient calculated from the amino acid sequence.[17] The purification yield of TrpE was 0.1 mg per liter cell suspension, and between 10 mg and 45 mg protein per liter cell suspension for the TrpGD and TrpG proteins.

**Steady-State Enzyme Kinetics.** The glutaminase activity of isolated TrpG was monitored at 25 °C by following glutamate production in a coupled enzymatic assay with bovine liver glutamate dehydrogenase (GDH, Sigma Aldrich) as the helper enzyme and $NAD^+$ as the coenzyme. A typical assay mixture contained 5 or 10 $\mu$M TrpG wild-type or variant protein, 5 mM $NAD^+$, 1 mg/mL GDH, and L-glutamine in 50 mM Tricine/KOH buffer pH 8.0. Glutamate produced by TrpG was oxidized by a molar excess of GDH yielding 2-oxoglutarate and NADH + $H^+$ + $NH_3$. The reaction was quantified by the increase in absorption at 340 nm, using $\Delta\varepsilon$(NADH-$NAD^+$) = 6300 $M^{-1}$ $cm^{-1}$. The anthranilate synthase activity of the TrpE−TrpG complex was assayed by measuring the formation of anthranilate at 40 °C. The incubation mixture contained 50 mM Tris/HCl pH 8.0, 2 mM $MgCl_2$, 57 $\mu$M chorismate, 0.25 $\mu$M TrpE, 0.75 $\mu$M TrpGD, and 0−60 mM L-glutamine. The reaction was started


dx.doi.org/10.1021/bi201618v | *Biochemistry* 2012, 51, 2812−2818

by the addition of chorismate and followed by the increase of anthranilate fluorescence at 400 nm (excitation at 350 nm). The values for $K_m^{Gln}$ and $V_{max}$ were determined by fitting a hyperbolic equation to saturation curves that were constructed on the basis of initial velocity measurements recorded in the presence of various concentrations of L-glutamine. The $k_{cat}$ values were calculated by dividing $V_{max}$ by the concentration of active sites ($[E_0]$).

**Radioactive Filter Binding Assay for Detection of the Thioester Intermediate.** A 100 μL assay mixture contained 50 mM Tricine/KOH pH 8.0, 80 μM wild-type or variant TrpG, 25 μL $^{14}$C-labeled glutamine (262 mCi/mmol), and 2 mM L-glutamine. Following incubation for 4 min at 25 °C, the reactions were quenched in 1 mL of 5% trichloracetic acid. After 2 min incubation in the quench solution, the precipitated enzyme−thioester complex was collected in microfilters (Whatman GF/C) by a vacuum device. The filters were subsequently washed with 30 mL of ice cold 1 N HCl and dried for 10 min at 60 °C. Trapped radioactivity which corresponds to the amount of formed thioester[18] was measured after incubation of the filters for 1 h in 5 mL of Lumasafe Plus (Lumac LSC) at room temperature in a Packard Tri-Carb 29000 TR scintillation counter. The given values are the mean of two independent measurements. Control experiments were performed under identical conditions in the absence of TrpG. The fraction of labeled protein was calculated by dividing the concentration of L-glutamine detected in the filters by total enzyme concentration.

**Following the Reaction of the Thioester Intermediate with Hydroxylamine.** A 4 M hydroxylamine stock solution, neutralized with solid NaOH to pH 7.4, was prepared fresh daily and kept on ice. Stop solution was mixed 1:1:1 from 80% TCA, 6 N HCl, and 10% $FeCl_3$ in 0.02 N HCl. *Qualitative assay*: 10 μM TrpG or TrpG-T129Y was incubated with 50 mM glutamine, 500 mM $NH_2OH$, and 50 mM potassium phosphate pH 7.5 in a volume of 800 μL at 37 °C. After 1 h the reaction was quenched with 200 μL of stop solution and centrifuged to remove particles. *Kinetics*: aliquots from a reaction mixture as described above were taken after several time intervals and quenched with stop solution. Following centrifugation, the amount of γ-glutamylhydroxamate formed was determined by measuring the absorbance at 540 nm of the hydroxamate-$FeCl_3$ complex which forms in acidic solution.[19] Commercially available γ-glutamylhydroxamate (Sigma Aldrich) was used as a standard.

**Molecular Dynamics (MD) Simulations.** The amino acid exchanges were introduced into TrpG employing the modeling suite Moloc[20] and initially minimized by using steepest decent minimization until an energy change per step below $10^{-4}$ kcal was reached. Subsequently, the proteins were heated to 298 K and equilibrated by Langevin-type dynamics (time step 2 fs) for 100 ps using the united atom force-field MAB[21] with implicit solvation. Water molecules found in the crystal structure forming H-bond networks at the protein surface within 12 Å from cysteine 83 were kept. Several independent production MD simulations with different starting geometries were performed at 298 K using Langevin-type dynamics (time step 2 fs) over 1 or 10 ns with one snapshot taken every 2 ps. Residues within 10 Å of the amino acid present at position 129 were free to move during the simulations and geometrically analyzed.

## RESULTS

We have studied activity regulation within the AS from the hyperthermophilic bacterium *Thermotoga maritima*, a complex between the synthase subunit TrpE and the glutaminase subunit TrpG fused to TrpD (anthranilate phosphoribosyl transferase), which catalyzes the second step in tryptophan biosynthesis. Our strategy to unravel the structural basis of regulated glutamine hydrolysis was to generate constitutively active TrpG variants, which produce ammonia independent of the presence of the TrpE synthase subunit. In order to identify candidate amino acids for mutation, we calculated a homology model of the TrpG domain of *T. maritima* TrpGD based on the crystal structure of TrpG from the hyperthermophile *S. solfataricus* (pdb-code 1QDL; 51% sequence identity).[13] TrpG from *T. maritima* was chosen as the model system instead of its structurally characterized homologues, because recombinant *S. solfataricus* TrpG is produced in *E. coli* with very low yields but we nevertheless wished to perform our mutational analysis with a robust protein scaffold from a hyperthermophile. Fitting of the TrpG model into the structure of the AS complex from *S. solfataricus* indicated that the sequence stretch L126-V127-A128-T129-R130-Y131 is localized between the catalytic triad Cys83−His175−Glu177 and the associated TrpE subunit (Figure 1). The stretch is partially conserved in the TrpG family (Figure S1) but not in other G-type glutaminases, and we hypothesized that its residues could be involved in the control of glutamine hydrolysis. Having in mind that marginal perturbations close to the active site can be sufficient for the stimulation of glutamine hydrolysis,[11] we replaced individual residues from this stretch and tested whether these exchanges lead to constitutive activity. In order to avoid the introduction of major conformational rearrangements and to minimize the risk of significant destabilization, we searched for homologous glutaminase subunits of another GATase with a corresponding stretch that could be transplanted into TrpG. This strategy is based on the high structural similarity between G-type glutaminases, which suggests that they have evolved from a common ancestor.[22] We chose HisH from *T. maritima* as donor glutaminase, because it is the nearest relative of TrpG among all available glutaminase structures. The HisH subunit and the associated HisF synthase subunit form the heterodimeric imidazoleglycerol phosphate synthase complex, a GATase involved in the biosynthesis of histidine.[8]

On the basis of the superposition of HisH and the TrpG homology model, we introduced the individual exchanges L126G, V127Y, T129Y, and Y131V into the background of the isolated TrpG domain (Figure 1; Figure S2). Residues A128 and R130 were not substituted as they do not point toward the TrpG−TrpE interface, which makes it unlikely that they are involved in the regulation of glutamine hydrolysis. The mutant genes were expressed in *E. coli*, and the TrpG variants were purified and tested for constitutive glutaminase activitiy using steady-state enzyme kinetics. The variants carrying the L126G and T129Y exchanges displayed measurable glutamine hydrolysis in the absence of TrpE (Figure 2A), whereas no constitutive activity was detected for wild-type TrpG and variants carrying the V127Y and Y131V substitutions (Table 1). In order to further analyze the requirements for constitutive glutamine hydrolysis at position 129, the TrpG variants T129F and T129A were also produced in *E. coli*, purified, and characterized by steady-state kinetics. The results showed that phenylalanine induces glutamine hydrolysis as effectively as

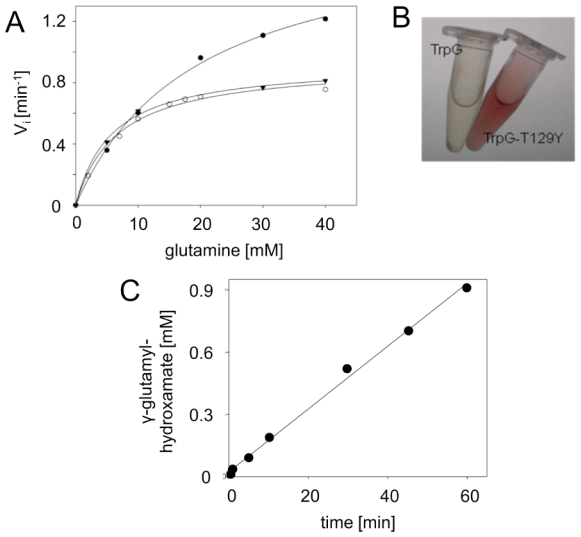


**Figure 2.** (A) Glutamine saturation curves of TrpG-T129Y (filled circles), TrpG-T129F (open circles), and TrpG-L126G (filled triangles). (B) Results of the assay for the qualitative detection of γ-glutamylhydroxamate performed with wild-type TrpG and TrpG-T129Y. (C) Time-dependent formation of γ-glutamylhydroxamate by TrpG-T129Y. The error of the data points corresponds approximately to the size of the symbols.

**Table 1. Steady-State Kinetic Parameters of TrpG Variants in Comparison to the AS Complex from *T. maritima*[a]**

| | $K_M^{Gln}$ [mM] | $k_{cat}$ [min$^{-1}$] | $k_{cat}/K_M^{Gln}$ [M$^{-1}$ s$^{-1}$] |
|---|---|---|---|
| TrpG wild-type | | no detectable activity | |
| TrpG-L126G | 5.8 ± 0.6 | 0.9 ± 0.03 | 2.6 |
| TrpG-V127Y | | no detectable activity | |
| TrpG-T129Y | 19.7 ± 1.8 | 1.8 ± 0.1 | 1.5 |
| TrpG-T129F | 6.6 ± 0.8 | 0.8 ± 0.04 | 2.0 |
| TrpG-T129A | | no detectable activity | |
| TrpG-Y131V | | no detectable activity | |
| TrpG-L126G-V127Y-T129Y-Y131V | 40.9 ± 2.9 | 1.6 ± 0.5 | 0.7 |
| AS | 1.5 ± 0.4 | 30 ± 1.3 | 333 |

[a]Experimental conditions: TrpG: 5 or 10 μM TrpG variant, 5 mM $NAD^+$, 1 mg/mL GDH, various concentrations of L-glutamine, 50 mM Tricine/KOH buffer pH 8.0 at 25 °C. No detectable activity: absence of measurable absorbance change in the presence of 20 μM TrpG variant and 40 mM glutamine over the course of several minutes. It follows that the $k_{cat}$-value must be lower than about 0.1 min$^{-1}$. AS: 0.25 μM TrpE, 0.75 μM TrpGD, 2 mM $MgCl_2$, 57 μM chorismate, various concentrations of L-glutamine, 50 mM Tris/HCl, pH 8.0 at 40 °C.

tyrosine, whereas alanine does not lead to measurable constitutive activity (Figure 2A; Table 1). To test if the activating effects of single exchanges would sum up, we also generated and characterized the quadruple variant TrpG-L126G+V127Y+T129Y+Y131V. However, this variant shows a similar catalytic activity as the TrpG variants that carry the single L126G or T129Y substitutions (Table 1), suggesting that these two exchanges activate the glutaminase via the same mechanism. As a reference for the constitutive glutaminase activities of our variants, the glutaminase activity of the AS complex, which was generated by mixing the recombinant TrpE and TrpGD subunits (Figure S3), was characterized by steady-state kinetics. The catalytic efficiency constant ($k_{cat}/K_M^{Gln}$) of the complex was elevated by about 2 orders of magnitude compared to the constitutively active TrpG variants, mainly as a consequence of a much higher turnover number (Table 1).

Glutamine hydrolysis by G-type glutamine amidotransferases occurs in two major steps.[23] The reaction is initiated by the nucleophilic attack of the thiolate anion of the catalytic cysteine onto the carboxamide group of glutamine, leading to the release of ammonia and the formation of a thioester intermediate. Then, the intermediate is decomposed by the nucleophilic attack of water, giving rise to glutamate and regenerating the free thiolate (Figure S4). We were interested to determine which of the two steps is rate-limiting for the constitutive glutaminase activity of the TrpG variants. For this purpose, glutaminase assays with TrpG and TrpG-T129Y were performed in the presence of hydroxylamine, which is a stronger nucleophile than water and therefore favorably competes with it for the reaction with the thioester intermediate. The reaction product is γ-glutamylhydroxamate which can be readily detected by its red color as a ferric complex in acidic solutions.[24] Whereas wild-type TrpG did not produce detectable amounts of γ-glutamylhydroxamate, TrpG-T129Y generated the alternate reaction product (Figure 2B), indicating that a significant concentration of the thioester is present in the steady-state. In accordance with this conclusion, a filter assay using radiolabeled glutamine showed that only 1.3% of the active sites of wild-type TrpG but 13.8% of TrpG-T129Y contained a covalently attached thioester under steady-state conditions. In order to determine whether the elevated thioester concentration of TrpG-T129Y is due to an increased rate of its formation or a decreased rate of its hydrolysis, we monitored the time-dependent formation of γ-glutamylhydroxamate by TrpG-T129Y in the presence of excess hydroxylamine (Figure 2C). The determined hydroxamate formation rate of 1.7 min$^{-1}$ matches the glutamine hydrolysis rate (1.8 min$^{-1}$), which is equivalent to $k_{cat}$ (Table 1). This accordance demonstrates that thioester formation is the rate-limiting step of the overall reaction.

In order to understand the structural basis for the different rates of thioester formation, we performed MD simulations. Despite serious efforts we were unable to crystallize the *T. maritima* TrpG domain, either as a single protein or as TrpGD fusion. Therefore we used homology models of wild-type TrpG and its constitutively active variants, which were based on the crystal structure of TrpG from *S. solfataricus*. Simulations performed over a time interval of 1 ns for constitutively active TrpG-L126G did not reveal any salient difference in comparison with the inactive wild-type TrpG and TrpG-T129A proteins. Position 126 is located remote from the active site at the root of a loop that spans the substrate binding cleft. Most probably the introduction of a glycine causes a significant structural rearrangement of the loop, which is not captured by our MD simulations of the L126G variant. However, for the constitutively active TrpG-T129F, TrpG-T129Y, and TrpG-L126G+V127Y+T129Y+Y131V variants a noticeable difference in the trajectories was observed, which reflects a reorientation of the catalytic dyad that leads to the reduction of the distance between the Cys83-Sγ and His175-N$\varepsilon_2$ atoms (Figure 3). For wild-type TrpG, TrpG-L126G, and TrpG-L126G+V127Y +T129Y+Y131V the distances were confirmed in elongated simulations over 10 ns (Figure S5). A minimal structural model deduced from the simulations suggests that the observed rearrangement of the two catalytic residues is caused by a closer packing of the loop covering the active site and favorable stacking interactions of His175 with the aromatic side chains of


dx.doi.org/10.1021/bi201618v | *Biochemistry* 2012, 51, 2812−2818

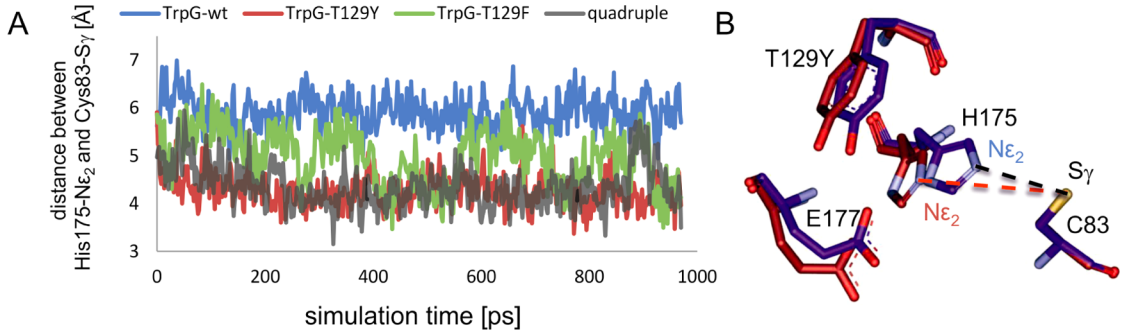


**Figure 3.** (A) Distance variation between Cys83-S$\gamma$ and His175-N$\varepsilon_2$ in the course of the MD simulations performed with wild-type TrpG, the variants carrying the single exchanges T129Y and T129F, and the quadruple variant L126G+V127Y+T129Y+Y131V. (B) TrpG catalytic triad at the beginning (red) and end (blue) of the MD simulation with TrpG-T129Y. Note that the imidazole ring of His175 rotates in the course of the simulation. As a consequence, the angle between the plane of the ring and Cys83-S$\gamma$ decreases, which increases the probability of proton transfer to His175-N$\varepsilon_2$.

the introduced Tyr129 or Phe129 residues. The comparison of the outcome of the MD simulations with the steady-state constants shows an inverse correlation of the H-bond distance between Cys83-S$\gamma$ and His175-N$\varepsilon_2$ and the turnover number for glutamine hydrolysis (Figure 4). The exception is

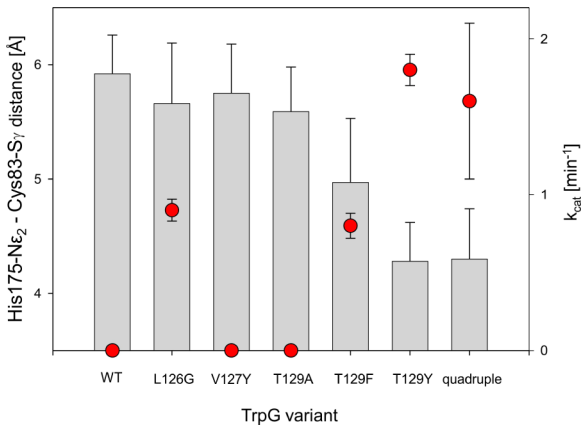


**Figure 4.** Distances between Cys83-S$\gamma$ and His175-N$\varepsilon_2$ at the end of the MD simulations (bars) and turnover numbers (red dots) of TrpG wild-type and variants carrying the indicated single exchanges, or the quadruple exchange L126G+V127Y+T129Y+Y131V.

TrpG-L126G, for reasons discussed above. This finding suggests that the deprotonation of Cys83 by His175, which initiates thioester formation, determines the rate of constitutive glutamine hydrolysis by TrpG.

## DISCUSSION

The crystal structures of several GATases have previously been analyzed to understand the signaling mechanisms leading to glutamine hydrolysis as a consequence of substrate binding to the synthase active site. These studies have demonstrated the requirement of ligand-induced conformational transitions for the proper formation of ammonia channels and the productive organization of the glutaminase active site.[2,25,26] Along the same lines, the crystal structures of the AS from *S. solfataricus* and *S. typhimurium* suggest that, in the absence of the TrpE-substrate chorismate, the conformation of the active site of TrpG does either not allow glutamine to enter or is catalytically incompetent due to local disorder.[13,14] Whereas these structures have not allowed for the proposal of a mechanism by which glutamine hydrolysis is stimulated at the active site of TrpG, our MD simulations indicate that the replacement of Thr129 by Phe or Tyr leads to glutaminase activation by reducing the distance between the active site Cys-His pair. It is plausible to assume that a similar rearrangement at the active site of TrpG occurs in the native AS complex as a consequence of ligand binding to TrpE. The decreased distance will facilitate proton transfer from the sulfhydryl group of Cys83 to the imidazole group of His175, and the resulting thiolate anion will then initiate a nucleophilic attack onto the carboxamide group of the glutamine side chain. The structure of the active AS from *S. marcescens*, which was crystallized in the presence of the TrpE substrate chorismate and the TrpG substrate glutamine,[15] supports this conclusion. It shows the catalytic triad of TrpG with the covalently bound thioester intermediate and a Cys-His distance of 3.5 Å. This distance is shorter by 0.7 Å than the Cys83−His175 distance of 4.2 Å modeled for TrpG-T129Y, in accordance with the significantly higher rate of glutamine hydrolysis of the AS complex in comparison to the constitutively active variant (Table 1). Remarkably, the Cys−His distance seems also to be crucial for the function of the main cysteine proteinase of SARS coronavirus: the two residues are separated 3.9 Å in the active dimer and by 4.4 Å in the inactive monomer.[27]

In order to further substantiate this finding, we analyzed the active sites of 20 cysteine protease structures deposited in the protein database and found a mean Cys−His distance of 3.7 ± 0.2 Å (Table S2, Supporting Information), which is remarkably close to the distance of 3.5 Å found in the active complex of *S. marcescens* AS. Along the same lines, a Cys−His H-bond distance between 3.1 Å and 4.2 Å was calculated in a quantum mechanical study dealing with proton transfer in an active cysteine protease.[28] It is further important to keep in mind that in a perfect catalytic orientation, the plane of the histidine imidazole side chain should be coplanar with the cysteine S$\gamma$ atom, which means that the H-bond network of the catalytic triad is ideally linear. In accordance with this notion, we observed an average Cys83-S$\gamma$−His175-N$\varepsilon_2$−Glu177-O$\varepsilon_2$ triad angle of about 17° in the simulations of TrpG-T129Y (Figure S6, Supporting Information), compared to 34° in the model of TrpG wild-type. Moreover, the crystal structures of the inactive forms of the AS complexes from *S. typhimurium* and *S. solfataricus* reveal H-bond distances between Cys to His of about 4 Å, but triad angles of 29° and 31°, respectively.[13,14] Remarkably, the low Cys−His distance of 3.1 Å in the inactive


dx.doi.org/10.1021/bi201618v | *Biochemistry* 2012, 51, 2812−2818

HisH protein from *T. maritima* (pdb-code 1k9v) would be compatible with efficient proton transfer, whereas the triad angle of 99° is highly unfavorable for catalysis. This finding suggests that the activation mechanism in the HisH−HisF imidazoleglycerol phosphate synthase complex also includes a rearrangement of the catalytic residues but differs in its atomic details from the activation mechanism in AS. Otherwise, the replacement of amino acids from TrpG with residues from HisH could not have led to constitutive glutamine hydrolysis.

Interestingly, the exchange of a cysteine with an aspartate residue (C248D) close to the active site of the glutaminase subunit of carbamoyl phosphate synthetase leads to a partial uncoupling of its hydrolytic activity from the presence of the synthetase substrates ATP and bicarbonate.[29] Although the crystal structure of this variant did reveal only minor alterations at the catalytic triad,[11] an activation mechanism similar to the one found in our TrpG variants might also be operational in carbamoyl phosphate synthetase. In contrast, the crystal structure of pyridoxalphosphate synthase from *Bacillus subtilis* points to an activation mechanism where complex formation between the synthase and glutaminase subunits generates an oxyanion hole that stabilizes the tetrahedral reaction intermediate.[10] The generation of constitutively active glutaminase variants of other GATases might help to decide whether activation mechanisms based on the rearrangement of the catalytic dyad or the proper formation of an oxyanion hole are more widespread among G-type glutaminases.

## ■ ASSOCIATED CONTENT

### Supporting Information

Table S1. Primers used for PCR amplification and plasmid cloning of *trp*E, *trp*GD, and *trp*G from *T. maritima*. Primers used for site-directed mutagenesis of *trp*G by overlap extension PCR. Table S2. Active site Cys-His distances in 20 different cysteine proteases. Figure S1. Multiple alignment of TrpG sequences. Figure S2. Stereo view of the active site in the homology model of TrpG from *T. maritima*. Figure S3. Analytical gel filtration runs of TrpE and TrpGD, and a mixture of TrpE with a molar excess of TrpGD. Figure S4. Reaction mechanism of glutamine hydrolysis by G-type glutaminases. Figure S5. Cys83-S$\gamma$−His75-N$\varepsilon_2$ distances determined in MD simulations with wild-type TrpG, TrpG-L126G, and TrpG-L126G+V127Y+T129Y+Y131V over 10 and 1 ns. Figure S6. Catalytic triad angle in TrpG-T129Y at the start and the end of an 1 ns MD simulation. Supplementary references. This material is available free of charge via the Internet at http://pubs.acs.org.

## ■ AUTHOR INFORMATION

### Corresponding Author

*Phone: +49-941-943 3015; fax: +49-941-943 2813; e-mail: Reinhard.Sterner@biologie.uni-regensburg.de.

### Notes

The authors declare no competing financial interest.

## ■ ACKNOWLEDGMENTS

We thank Frank Raushel (Texas A&M University), Sandra Schlee, and Monika Meier (University of Regensburg) for comments on the manuscript.

## ■ ABBREVIATIONS

AS, anthranilate synthase; TrpE, synthase subunit of AS; TrpG, glutaminase subunit of AS; TrpD, anthranilate phosphoribosyl transferase; GATase, glutamine amidotransferase

## ■ REFERENCES

(1) Massiere, F., and Badet-Denisot, M. A. (1998) The mechanism of glutamine-dependent amidotransferases. *Cell. Mol. Life Sci. 54*, 205−222.

(2) Mouilleron, S., and Golinelli-Pimpaneau, B. (2007) Conformational changes in ammonia-channeling glutamine amidotransferases. *Curr. Opin. Struct. Biol. 17*, 653−664.

(3) Raushel, F. M., Thoden, J. B., and Holden, H. M. (1999) The amidotransferase family of enzymes: molecular machines for the production and delivery of ammonia. *Biochemistry 38*, 7891−7899.

(4) Zalkin, H., and Smith, J. L. (1998) Enzymes utilizing glutamine as an amide donor. *Adv. Enzymol. Relat. Areas Mol. Biol. 72*, 87−144.

(5) Ollis, D. L., Cheah, E., Cygler, M., Dijkstra, B., Frolow, F., Franken, S. M., Harel, M., Remington, S. J., Silman, I., Schrag, J., et al. (1992) The $\alpha/\beta$ hydrolase fold. *Protein Eng. 5*, 197−211.

(6) Brannigan, J. A., Dodson, G., Duggleby, H. J., Moody, P. C., Smith, J. L., Tomchick, D. R., and Murzin, A. G. (1995) A protein catalytic framework with an N-terminal nucleophile is capable of self-activation. *Nature 378*, 416−419.

(7) Huang, X., Holden, H. M., and Raushel, F. M. (2001) Channeling of substrates and intermediates in enzyme-catalyzed reactions. *Annu. Rev. Biochem. 70*, 149−180.

(8) Beismann-Driemeyer, S., and Sterner, R. (2001) Imidazole glycerol phosphate synthase from *Thermotoga maritima*. Quaternary structure, steady-state kinetics, and reaction mechanism of the bienzyme complex. *J. Biol. Chem. 276*, 20387−20396.

(9) Miles, B. W., Banzon, J. A., and Raushel, F. M. (1998) Regulatory control of the amidotransferase domain of carbamoyl phosphate synthetase. *Biochemistry 37*, 16773−16779.

(10) Strohmeier, M., Raschle, T., Mazurkiewicz, J., Rippe, K., Sinning, I., Fitzpatrick, T. B., and Tews, I. (2006) Structure of a bacterial pyridoxal 5′-phosphate synthase complex. *Proc. Natl. Acad. Sci. U. S. A. 103*, 19284−19289.

(11) Thoden, J. B., Huang, X., Kim, J., Raushel, F. M., and Holden, H. M. (2004) Long-range allosteric transitions in carbamoyl phosphate synthetase. *Protein Sci. 13*, 2398−2405.

(12) Morollo, A. A., and Bauerle, R. (1993) Characterization of composite aminodeoxyisochorismate synthase and aminodeoxyisochorismate lyase activities of anthranilate synthase. *Proc. Natl. Acad. Sci. U. S. A. 90*, 9983−9987.

(13) Knöchel, T., Ivens, A., Hester, G., Gonzalez, A., Bauerle, R., Wilmanns, M., Kirschner, K., and Jansonius, J. N. (1999) The crystal structure of anthranilate synthase from *Sulfolobus solfataricus*: functional implications. *Proc. Natl. Acad. Sci. U. S. A. 96*, 9479−9484.

(14) Morollo, A. A., and Eck, M. J. (2001) Structure of the cooperative allosteric anthranilate synthase from *Salmonella typhimurium*. *Nat. Struct. Biol. 8*, 243−247.

(15) Spraggon, G., Kim, C., Nguyen-Huu, X., Yee, M. C., Yanofsky, C., and Mills, S. E. (2001) The structures of anthranilate synthase of *Serratia marcescens* crystallized in the presence of (*i*) its substrates, chorismate and glutamine, and a product, glutamate, and (*ii*) its end-product inhibitor, L-tryptophan. *Proc. Natl. Acad. Sci. U. S. A. 98*, 6021−6026.

(16) Ho, S. N., Hunt, H. D., Horton, R. M., Pullen, J. K., and Pease, L. R. (1989) Site-directed mutagenesis by overlap extension using the polymerase chain reaction. *Gene 77*, 51−59.

(17) Pace, C. N., Vajdos, F., Fee, L., Grimsley, G., and Gray, T. (1995) How to measure and predict the molar absorption coefficient of a protein. *Protein Sci. 4*, 2411−2423.

(18) Lusty, C. J. (1992) Detection of an enzyme bound gamma-glutamyl acyl ester of carbamyl phosphate synthetase of *Escherichia coli*. *FEBS Lett. 314*, 135−138.

(19) Woolfolk, C. A., Shapiro, B., and Stadtman, E. R. (1966) Regulation of glutamine synthetase. I. Purification and properties of glutamine synthetase from *Escherichia coli*. *Arch. Biochem. Biophys. 116*, 177−192.
(20) Gerber, P. R., and Müller, K. (1995) MAB, a generally applicable molecular force field for structure modelling in medicinal chemistry. *J. Comput.-Aided Mol. Des. 9*, 251−268.
(21) Gerber, P. R. (1998) Charge distribution from a simple molecular orbital type calculation and non-bonding interaction terms in the force field MAB. *J. Comput.-Aided Mol. Des. 12*, 37−51.
(22) Zalkin, H. (1993) The amidotransferases. *Adv. Enzymol. Relat. Areas Mol. Biol. 66*, 203−309.
(23) Thoden, J. B., Miran, S. G., Phillips, J. C., Howard, A. J., Raushel, F. M., and Holden, H. M. (1998) Carbamoyl phosphate synthetase: caught in the act of glutamine hydrolysis. *Biochemistry 37*, 8825−8831.
(24) Chaparian, M. G., and Evans, D. R. (1991) The catalytic mechanism of the amidotransferase domain of the Syrian hamster multifunctional protein CAD. Evidence for a CAD-glutamyl covalent intermediate in the formation of carbamyl phosphate. *J. Biol. Chem. 266*, 3387−3395.
(25) Li, Q. A., Mavrodi, D. V., Thomashow, L. S., Roessle, M., and Blankenfeldt, W. (2011) Ligand binding induces an ammonia channel in 2-amino-2-desoxyisochorismate (ADIC) synthase PhzE. *J. Biol. Chem. 286*, 18213−18221.
(26) Mouilleron, S., Badet-Denisot, M. A., and Golinelli-Pimpaneau, B. (2008) Ordering of C-terminal loop and glutaminase domains of glucosamine-6-phosphate synthase promotes sugar ring opening and formation of the ammonia channel. *J. Mol. Biol. 377*, 1174−1185.
(27) Tan, J., Verschueren, K. H., Anand, K., Shen, J., Yang, M., Xu, Y., Rao, Z., Bigalke, J., Heisen, B., Mesters, J. R., Chen, K., Shen, X., Jiang, H., and Hilgenfeld, R. (2005) pH-dependent conformational flexibility of the SARS-CoV main proteinase (M(pro)) dimer: molecular dynamics simulations and multiple X-ray structure analyses. *J. Mol. Biol. 354*, 25−40.
(28) Mladenovic, M., Fink, R. F., Thiel, W., Schirmeister, T., and Engels, B. (2008) On the origin of the stabilization of the zwitterionic resting state of cysteine proteases: a theoretical study. *J. Am. Chem. Soc. 130*, 8696−8705.
(29) Mareya, S. M., and Raushel, F. M. (1994) A molecular wedge for triggering the amidotransferase activity of carbamoyl phosphate synthetase. *Biochemistry 33*, 2945−2950.